Theoretical investigation of He^{2+}-Ar collisions in the energy range of 4–300 keV/amu

C. L. Zhang,[1,2] X. H. Hong,[3] F. Wang,[4] Y. Wu,[2] and J. G. Wang[2]

[1]*Electric and Information Engineering College, Xuchang University, Xuchang 461000, People's Republic of China*

[2]*Institute of Applied Physics and Computational Mathematics, P. O. Box 8009, Beijing 100088, People's Republic of China*

[3]*School of Physics, Key Laboratory of Cluster Science of Ministry of Education, Beijing Institute of Technology, Beijing 100081, People's Republic of China*

[4]*Laser Micro/Nano Fabrication Laboratory, School of Mechanical Engineering, Beijing Institute of Technology, Beijing 100081, People's Republic of China*

(Received 19 December 2012; revised manuscript received 13 February 2013; published 19 March 2013; corrected 21 March 2013)

The time-dependent density functional theory is applied to investigate the charge transfer and electron-loss processes during He^{2+}-Ar collisions in the energy range of 4–300 keV/amu. A coordinate space translation technique is employed to focus our investigation on some certain space of interest such as the regions around the projectile or target. It is shown that both charge transfer and electron-loss processes are important in the considered energy range. One-electron-capture processes dominate charge transfer with the cross sections one to two orders of magnitude larger than two-electron-capture cross sections. The ionization cross sections decrease with increasing the number of ionized electrons. The calculated cross sections are in excellent agreement with available experimental and theoretical results. Evolution of electron density is also presented to explore interactions between the electrons as well as the correlation between the projectile and target during the collisions.

DOI: 10.1103/PhysRevA.87.032711 PACS number(s): 34.10.+x, 34.70.+e, 34.50.Fa

I. INTRODUCTION

Heavy particle collisions (HPCs) play an important role in laboratory and astrophysical plasma environments by affecting the ionization balance and energy transport when the electron density and temperature are low. For its importance in related fields and the complex dynamics, HPCs have been extensively investigated [1,2] both experimentally and theoretically, but they are still a challenging subject due to the multicenter and the strong electron correlation effects, especially in the low and intermediate collision energy range.

A number of theoretical methods have been proposed, developed, and successfully applied to treat the HPC processes in various energy ranges. The molecular-orbital close-coupling method has been successfully applied to treat multielectron collision processes in the low-energy range [3–6]. It describes the electron (and sometimes nuclear) dynamics fully quantally, but cannot effectively treat the ionization processes. The atomic-orbital close-coupling method has been widely used to deal with intermediate energy collisions, but this method is essentially a quasi-one-electron model and just appropriate for those systems in which the atomic structure can be described reasonably with the use of a model potential, for example, the collision system including highly charged ions [7,8]. The classical trajectory Monte Carlo (CTMC) technique has also been applied to investigate the high-energy collisions. However, the quantum effects have been partially lost by classical treatment of the CTMC method [9]. Similarly, the continuum distorted-wave (CDW) method is just reasonable for high-energy collisions. The time-dependent Schrödinger equation (TDSE) method has been proposed and can obtain all the dynamics information for the whole ion-atom collision processes, but it is just applicable for quasi-one-electron systems due to the rapid increasing of the computational cost with the number of active electrons [10,11].

In this work, a time-dependent density function theory (TDDFT) has been developed and applied to study He^{2+}-Ar collisions. We have computed charge transfer and electron-loss cross sections which are, among others, necessary physical parameters in the simulations of particle transport and energy transfer in the diverter region of Tokamak. Namely, He^{2+} is the product of deuterium-tritium fusion and Ar is often used for the diagnostics or as a cooling, buffer gas in the diverter. For its importance in the research of magnetic fusion energy, He^{2+}-Ar collision has been investigated widely by many groups. Theoretically, the single-electron-capture cross sections have been calculated by CDW approximation for 188–6250 keV/amu, but the double-electron-capture cross sections have not been obtained yet [12]. The electron-loss cross sections have been calculated by a time-dependent independent-particle model (TDIPM) in the energy range of 5–1000 keV/amu [13]. The results obtained by taking into account the effect of the target response agree with the experimental data. The absolute total cross sections have been measured in the energy range of 50–250 keV/amu [14]. Cross sections for the production of positive and negative charges with 10–300 keV/amu He^{2+} ion on argon were measured by the transverse-field method [15]. DuBois presented measurements of absolute cross sections for multiple ionization of argon by 50–500 keV/amu He^{2+} [16].

This paper is organized as follows. In Sec. II, the theoretical and computational method is summarized. The results and discussion are presented in Sec. III. Our conclusions are given in Sec. IV. Atomic units are used throughout the paper unless indicated.

II. THEORETICAL AND COMPUTATIONAL METHOD

The TDDFT method has been described thoroughly in previous works [17–19] and we only briefly discuss it here. In principle, all dynamic information of ion-atom collisions can be obtained by using the TDSE method. However, the TDSE for a multielectron system is difficult to solve accurately due to a large number of degrees of freedom and coupled

equations, and thus excessive computational cost. In the TDDFT model, the coupled multielectron TDSE is replaced by a set of time-dependent Kohn-Sham equations, which yield directly the time-dependent electron density of the multielectron system [20]. In the present work, the TDDFT formalism was implemented on real-space grids following the OCTOPUS program [21]. A high-order finite difference method with nine-point formula was applied to the Laplacian operation of Perdew-Zunger's exchange-correlation function [22,23]. The Troullier-Martins' pseudopotential [24] in the separable Kleinman-Bylander form [25] has been used in the present calculations in the same way as was done by Wang *et al.* [17]. In the He^{2+}-Ar($3s^2 3p^6$) system, initially eight valence electrons populate the $3s$, $3p_1$, $3p_0$, and $3p_{-1}$ orbitals of the target atom. The Kohn-Sham equation is

$$i\frac{\partial\varphi_{k\mu}(\vec{r},t)}{\partial t} = \hat{H}_{\mathrm{KS}}\varphi_{k\mu}(\vec{r},t) = \left[-\frac{1}{2}\nabla^2 + V_{\mathrm{KS}}(\vec{r},t)\right]\varphi_{k\mu}(\vec{r},t), \tag{1}$$

where $\varphi_{k\mu}(\vec{r},t)$ is the Kohn-Sham orbital (KSO). Using the orthogonal relations of the KSO, the density can be written as

$$\rho(\vec{r},t) = \sum_{\mu=\uparrow\downarrow}\rho_\mu(\vec{r},t) = \sum_{\mu=\uparrow\downarrow}\sum_{k=1}^{4} n_{\mu k}|\varphi_{k\mu}(\vec{r},t)|^2. \tag{2}$$

The Slater determinant Φ can be obtained from the KSOs:

$$\Phi = \frac{1}{\sqrt{N!}}\det|\varphi_{3s\uparrow}\varphi_{3s\downarrow}\varphi_{3p_1\uparrow}\varphi_{p_1\downarrow}\varphi_{3p_0\uparrow}\varphi_{3p_0\downarrow}\varphi_{3p_{-1}\uparrow}\varphi_{3p_{-1}\downarrow}|, \tag{3}$$

where $\uparrow$ (or $\downarrow$) indicates a spin-up (or spin-down) orbital and $n_{k\mu}$ is the occupation number. Using the generalized Lüdde and Dreizler's formulation [26] of Wang *et al.* [17], the electron-capture probability and the electron-loss probability are calculated by

$$p_{i,j}(b) = \binom{N}{n=i-j}\int_T d\vec{r}_1,\ldots,d\vec{r}_n\int_{\bar{T}} d\vec{r}_{n+1},\ldots, d\vec{r}_N|\Phi(\vec{r}_1,\ldots,\vec{r}_N,t_f;b)|^2, \tag{4}$$

$$p_q(b) = \binom{N}{m=N-q}\int_T d\vec{r}_1,\ldots,d\vec{r}_m\int_{\bar{T}} d\vec{r}_{m+1},\ldots, d\vec{r}_N|\Phi(\vec{r}_1,\ldots,\vec{r}_N,t_f;b)|^2, \tag{5}$$

where i and j are the ionic states of the projectile before and after collision. N is the total number of electrons on the target before collision, $n = i - j$ is the number of electrons transferred to the projectile, and q is the degree of ionization. Here T represents the spatial area around the projectile or target and $\bar{T}$ is the spatial area outside it, and $\vec{r}_l$ denotes spatial and spin coordinates of the lth electron.

In principle, the full evolution space should be considered to obtain complete dynamic information of the collision process. However, only the region around the projectile or the target is necessary to obtain the electron capture or electron-loss probability in real calculations due to the fact that the simulation box size is limited to a small size. In the present work, the coordinate space translation (CST) technique is used to move all nuclei and electron coordinates into the simulation box [17]. The CST technique allows one to focus on a certain space of interest such as the region around the projectile. After the collision process, in order to obtain the electron-loss probability for electron-capture processes, the simulation box is centered on the target and only the spatial area around the target is needed; while for the case of electron capture, the CST technique is adopted and the simulation box is centered on the projectile and only the space around the projectile is needed. For a given incident energy and impact parameter b, the electron-capture or electron-loss cross section is determined by

$$\sigma = 2\pi\int p(b)b\,db. \tag{6}$$

In the present collision geometry, the x–y plane is chosen as the scattering plane. The target is initially placed at the center of the simulation box, while the projectile is initially separated from the target in the x direction with an impact parameter b along the y axis, with a velocity parallel to the x axis toward the target, as shown in Fig. 1(a). Figure 1(b) shows that the positions of the projectile and target along the x axis and y axis with the impact energy of 10 keV/amu and impact parameter of 2 a.u. The initial coordinates of projectile and target are (−10,2) and (0,0), respectively. The positions are translated 2 a.u. along the negative y direction as the projectile comes to the nearest point to the target. Then the coordinates of the projectile and target are (0,0) and (0,−2), respectively. After the translation mechanism is turned on, the position of the projectile is translated to reference point (5,0) when the distance of the projectile with reference point is larger than 3 a.u., and the target is removed synchronously from the left of the simulation box. When the distance between the target and projectile approaches 40 a.u. in the x direction, the collision process is considered to be over in real simulation, since the charge transfer or electron-loss probabilities become negligible in the regime of larger impact parameters.

After the collision processes there is a reprocessing together with an absorbing potential [27], but only for the case when the projectile or the target is in the simulation box. As a result of long-time evolution the fraction of the wave function associated with highly excited or continuum states can be removed by the complex absorbing potential. This ensures that the electron (around the projectile or target) number remains conserved and no free electron presents in the integral volume.

III. RESULTS AND DISCUSSION

The He^{2+}-Ar collision has been investigated using the TDDFT method in an energy range of 4–300 keV/amu and the following processes have been included:

$$He^{2+} + Ar \rightarrow He^{+} + Ar^{q+} + (q-1)e, \quad \text{single capture}, \tag{7}$$

$$He^{2+} + Ar \rightarrow He + Ar^{q+} + (q-2)e, \quad \text{double capture}, \tag{8}$$

$$He^{2+} + Ar \rightarrow He^{2+} + Ar^{q+} + qe, \quad \text{direct ionization}. \tag{9}$$

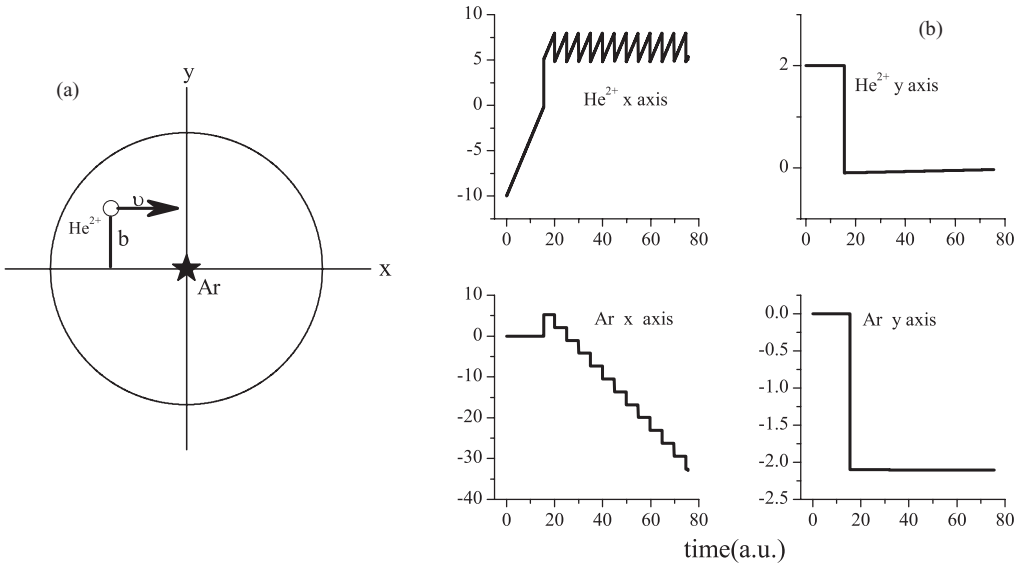

FIG. 1. (a) The initial position of the projectile and target. (b) The positions evolution of the projectile and target at the x direction and y direction with the incident energy of 10 keV/amu and impact parameter of 2 a.u.

In the present TDDFT calculations, the simulation box is spheriform with the maximum radius 25 a.u. The grid spacing is $\Delta x = \Delta y = \Delta z = 0.35$ a.u., and the time step is $\Delta t = 0.025$ a.u., which ensures a stable time evolution. It should be noted that the simulation box sizes and the spatial and time steps adopted in the simulation have been tested and ensure that all obtained cross sections converge well and with a reasonable computing cost at the same time.

The time-dependent methods have a natural advantage to obtain an insight in the time-dependent collision process. In Fig. 2, the evolutions of electronic density distribution in the $z = 0$ scattering plane are presented. In Fig. 2(a), the incident He^{2+} ion comes from the top left and the target Ar is located at the center of the real-space simulation box. While the projectile approaches, the electron cloud around the target is distorted considerably and a quasimolecular configuration is formed, as shown in Fig. 2(b). The CST technique is applied to focus on the region around the projectile. From Fig. 2(c), the target moves backward in the fame out of the simulation box.

The electron cloud around the target is absorbed when reaching the boundary due to the absorbing boundary condition. The electron cloud around the target is vortical in Figs. 2(b)–2(f) when the projectile approaches and leaves. So Fig. 3 gives the long-time evolution of the electronic density around the target as the projectile leaves the simulation box, where the electron number remains conserved and the electron density distribution varies periodically, i.e., there is no interaction when the collision process is over.

Using Eqs. (4) and (5), the probabilities $2\pi pb$ of electron capture and electron loss are calculated and plotted in Figs. 4(a) and 4(b), respectively, as a function of impact parameter for a collision energy of 10 keV/amu. It is shown that both electron-capture and electron-loss probabilities converge to zero as the impact parameter increases to ∼9 a.u., which indicates that the maximum impact parameter of 10 a.u is sufficiently large in the present calculation.

In Fig. 5, the electron-capture cross sections are presented and compared with the available theoretical and experimental data [15,28–35]. It is shown that the one-electron-capture cross sections are about one order of magnitude larger than the two-electron-capture cross sections. There is excellent agreement with all available measurements in this case, except for a small difference at a few lowest and highest energy

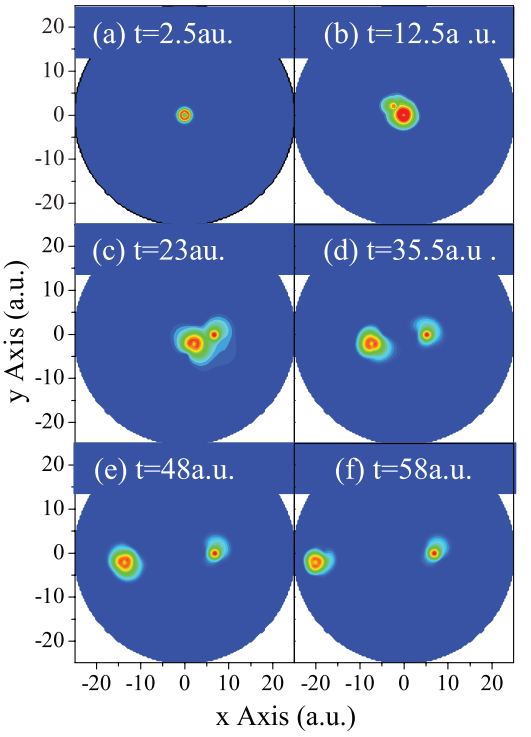

FIG. 2. (Color online) Evolution of the electron density around the projectile and target at an incident energy of 10 keV/amu and impact parameter of 2 a.u. Note that the contour is plotted in the $z = 0$ scattering plane. The scale of the electron density is logarithmic.

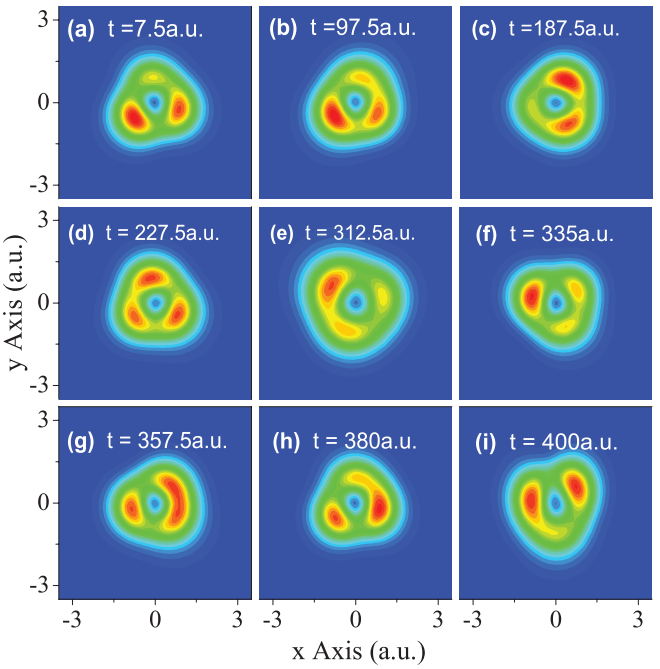

FIG. 3. (Color online) Long-time evolution of electron density around the target as the projectile leaves the simulation box for an incident energy of 10 keV/amu and impact parameter of 2 a.u. Note that the contour is plotted in the $z = 0$ scattering plane.

points. The discrepancy at very low energies is due to the used pseudopotential which cannot accurately describe the strong electron correlation. The discrepancy at very high energies is possibly due to insufficiently fine spatial and temporal numerical meshes. Compared to the experimental data, our results are much better than the theoretical results of Belkić *et al.* [12]. For two-electron capture, the cross sections from our calculation are also in good agreement with the available experimental data except at very low impact energy 4 keV/amu, which is likely due to the lack of quality of the pseudopotential to describe the strong electron correlation. It should be noted that at very low energies, the total charge transfer cross sections of the one-electron and two-electron capture obtained from our calculation are in very good agreement with the experimental results. In the present calculation, the K- and L-shell electrons are represented by a pseudopotential, which cannot describe the K- and L-shell contribution effectively when energy is very high and inner-shell electron ionization processes become important. The Auger processes following the inner-shell vacancy creation may change the recoil charge state distribution when energy is very high, and this partly explains the discrepancy between the present TDDFT calculation and the measurement in Fig. 5 for energies greater than 200 keV/u [13].

The net electron-loss cross sections in He^{2+}-Ar collision processes have also been calculated. The electron loss is produced by two main physical processes: direct ionization and the capture ionization given by formulas (7), (8), and (9), respectively. The total electron-loss cross section is the sum of electron-loss cross sections of different ionization degree ($q = 1,8$). The total electron-loss cross section is shown in Fig. 6 together with the experimental results of Rudd *et al.* [15] and DuBois *et al.* [16] and the TDIPM results of Kirchner *et al.* [13] for comparison. In the energy range considered here, the present TDDFT results are in good agreement with both the experimental data [15,16] and the other theoretical results [13] in that case when the latter theory takes into account the time-dependent screening defects of the target (response). The no-response calculation overestimates experiment at the broad maximum by 30%. This indicates that both TDDFT and TDIPM with target response are reliable for calculations of the total electron-loss cross section. It is also shown that, compared with the measurement of DuBois *et al.*, our calculation is much better than the TDIPM calculations with target response of Kirchner *et al.* at low energies of about a few keV/amu, which indicates that the TDDFT method is more reliable at low energies and TDIPM cannot account for the strong electron correlation effect sufficiently [36].

In Fig. 7, the cross sections of Ar^{q+} are shown for a number of ionization degrees q ($q = 1$–5) together with the experimental results of DuBois and Andersen *et al.* [16,37] as well as the theoretical results of Kirchner *et al.* [13] for comparison. For each q, the electron-loss cross sections vary

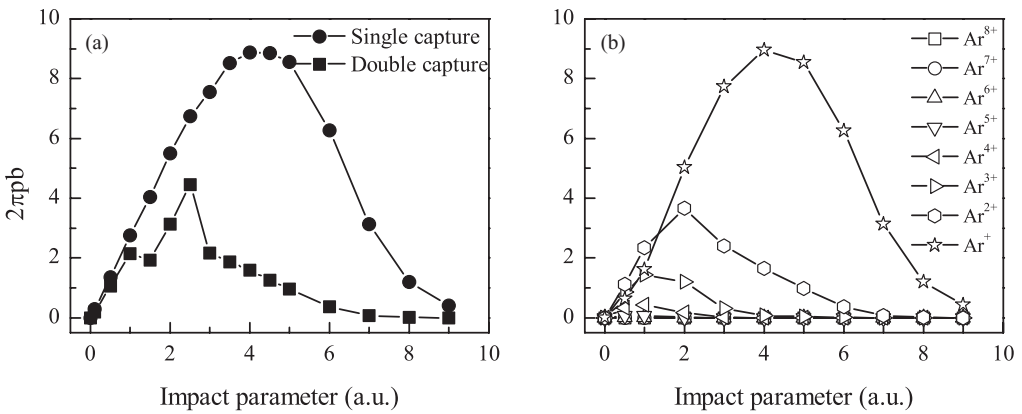

FIG. 4. (a) Probability of electron capture as a function of impact parameter at an incident energy of 10 keV/amu. Closed circles, single-electron capture; closed squares, double-electron capture. (b) Probability of electron loss for various ionization degrees ($q = 1$–8) as a function of impact parameter at an incident energy of 10 keV/amu.

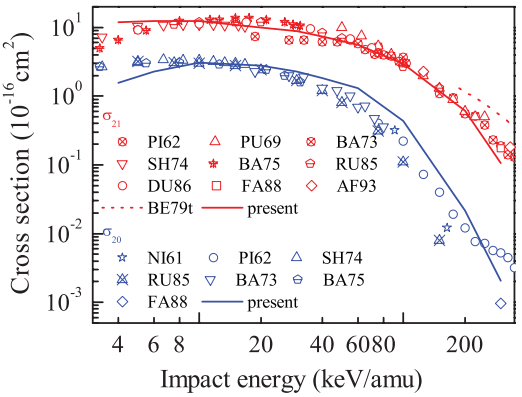

FIG. 5. (Color online) The present cross sections of single-electron capture (red line) and two-electron capture (blue line), together with experimental [15,28–35] and theoretical (BE79t [12]) results.

slowly with the variation of the incident energy. At the same time, at a fixed incident energy the cross sections decrease strongly with the increasing of ionization degree q. For $q \geqslant 6$, the electrons-loss cross sections are negligible and are not shown in Fig. 7 for clarity of the figure. For $q = 1$, in the energy range considered here, the incident energy of the He^{2+} ion approaches the bound energies of the active electrons of Ar^{q+} and thus the electrons are easily captured or ionized. With the increase of q, the bound energies of the active electrons of Ar^{q+} become so high that it is difficult to ionize the electrons by the low-energy He^{2+}. For $q = 1$, our results are consistent with both the theoretical TDIPM results (target response) of Kirchner *et al.* and the experimental results. For $q = 2$, good agreement between our results and all the other available results is achieved except for the theoretical results of Kirchner *et al.* in the energy range of 10–30 keV/amu, which are also larger than all the experimental results. For $q = 3$, there is good agreement with the measurement except for energies below 20 keV/amu. This is possibly due to the insufficient description of the electron correlation by the applied pseudopotential. Furthermore, compared with the

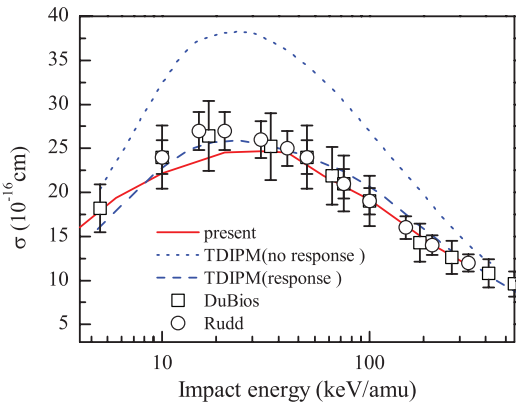

FIG. 6. (Color online) Total cross section for the net electron loss as a function of the impact energy. The red solid line is the result of the present work, the open squares and circles are experimental results [15,16], and the blue dashed line (target response) and the blue dotted line (no response) are the results of TDIPM theory [13].

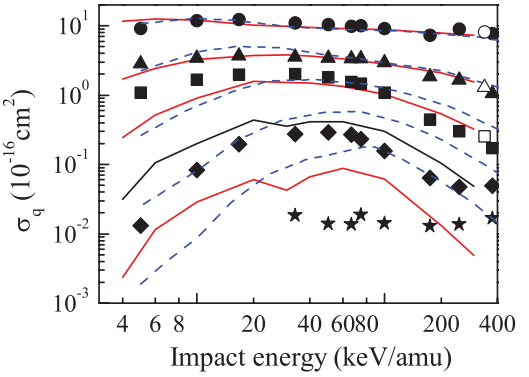

FIG. 7. (Color online) Total cross sections for q-fold electron loss σ_q ($q = 1$–5) as functions of impact energy. Theory: red (solid) lines (present calculations) and blue (dashed) lines [13] correspond to $q = 1$, 2, 3, 4, and 5 from top to bottom. Experiment: closed symbols [16] and open symbols [37]. Circles, $q = 1$; triangles, $q = 2$; squares, $q = 3$; diamonds, $q = 4$; stars, $q = 5$.

experimental results our calculation is much better than the calculation of Kirchner *et al.* in the whole energy range. For $q = 4$, there are obvious discrepancies in magnitude between calculations and measurements, while all results are in a similar trend with the change of the incident energy. This indicates that both the TDDFT and TDIPM have not taken good care of the strong electron correlation effect in this case. For $q = 5$, both calculations increase and then decrease with incident energy, while the measurement of DuBois *et al.* is nearly constant. This may partly be due to the insufficient description of the electron correlation in the calculations. This may also be caused by the fact that the electron-loss cross sections σ_5 are too small to be measured effectively. High precision measurement is expected to test the present calculation as a benchmark.

Some effects cannot be described by the present TDDFT method, including the effect of autoionization of the target or projectile following the double excitation of the target or double capture into excited states of the projectile, the effect of the Auger processes following the inner-shell vacancy creation, and the strong electron correlation effect in the collision processes at very low energies. The pseudopotential adopted in the TDDFT simulation is not suitable for the treatment of processes leading to very high excited states, the inner-shell electron ionization, and the strong electron correlation.

IV. CONCLUSIONS

The TDDFT method together with the CST technique has been applied to investigate He^{2+}-Ar collisions. Over the collision energy range of 4–300 keV/amu, the charge capture and the electron-loss processes are dominant. The cross sections of charge capture and electron loss have also been calculated. The charge capture processes include one-electron capture and two-electron capture, and the electron loss includes the direct ionization and capture ionization. The cross sections of charge capture and electron loss obtained from the present TDDFT calculations are in good agreement with the available experimental data and are better than the available

theoretical results. This demonstrates that the TDDFT is an effective method to treat HPCs of multielectron systems in medium to high energies. On the other hand, for low incident energies less than a few keV/amu, the electron correlation effect becomes too strong and cannot be described effectively in the TDDFT method. Despite the success of TDDFT in treating the electron-capture and electron-loss processes of a multielectron system, there are still obvious discrepancies between the present TDDFT calculation and measurements at energies less than a few keV/amu, especially for Ar^{q+} with $q \geqslant 4$. High precision theoretical results and experimental data are expected to provide a more reliable benchmark so as to further check the present TDDFT and future theoretical investigation.

ACKNOWLEDGMENTS

This work was supported by The National Natural Science Foundation of China (Grants No. 1102541 and No. 1120417), the National Basic Research program of China (Grant No. 2013CB922200), Defense Industrial Technology Development Program (Grant No. B1520110011), and Science and Technology Funds of China Academy of Engineering Physics (Grant No. 2012B0102015).

[1] J. W. Hooper, E. W. Mcdaniel, D. W. Martin, and D. S. Harmer, Phys. Rev. **121**, 1123 (1961).
[2] R. A. Langley, D. W. Martin, D. S. Harmer, J. W. Hooper, and E. W. Mcdaniel, Phys. Rev. **136**, A379 (1964).
[3] W. Fritsch and C. D. Lin, Phys. Rep. **202**, 1 (1991).
[4] A. R. Turner, D. L. Cooper, J. G. Wang, and P. C. Stancil, Phys. Rev. A **68**, 012704 (2003).
[5] R. Rejoub, M. E. Bannister, C. C. Haverner, D. W. Savin, C. J. Verzani, J. G. Wang, and P. C. Stancil, Phys. Rev. A **69**, 052704 (2004).
[6] L. B. Zhao, D. C. Joseph, B. C. Saha, H. P. Liebermann, P. Funke, and R. J. Buenker, Phys. Rev. A **79**, 034701 (2009).
[7] L. Liu, C. H. Liu, J. G. Wang, and R. K. Janev, Phys. Rev. A **84**, 032710 (2011).
[8] L. Liu, J. G. Wang, and R. K. Janev, Phys. Rev. A **77**, 042712 (2008).
[9] P. C. Stancil *et al.*, J. Phys. B **31**, 3647 (1998).
[10] D. R. Schultz, P. S. Krstić, C. O. Reinhold, and J. C. Wells, Phys. Rev. Lett. **76**, 2882 (1996).
[11] D. R. Schultz, J. C. Wells, P. S. Krstić, and C. O. Reinhold, Phys. Rev. A **56**, 3710 (1997).
[12] Dž. Belkić, R. Gayet, and A. Salin, Phys. Rep. **56**, 279 (1979).
[13] T. Kirchner, M. Horbatsch, and H. J. Lüdde, Phys. Rev. A **66**, 052719 (2002).
[14] L. J. Puckett, G. P. Taylor, and D. W. Martin, Phys. Rev. **178**, 271 (1969).
[15] M. E. Rudd, T. V. Goffe, and A. Itoh, Phys. Rev. A **32**, 2128 (1985).
[16] R. D. DuBois, Phys. Rev. A **36**, 2585 (1987).
[17] F. Wang, X. H. Hong, J. Wang, and K. S. Kim, J. Chem. Phys. **134**, 154308 (2011).
[18] F. Wang, X. C. Xu, X. H. Hong, J. Wang, and B. C. Gou, Phys. Lett. A **375**, 3290 (2011).
[19] F. Wang, X. H. Hong, J. Wang, B. C. Gou, and J. G. Wang, Phys. Lett. A **376**, 469 (2012).
[20] E. Runge and E. K. U. Gross, Phys. Rev. Lett. **52**, 997 (1984).
[21] M. A. L. Marques, A. Castro, G. F. Bertsch, and A. Rubio, Comput. Phys. Commun. **151**, 60 (2003).
[22] J. R. Chelikowsky, N. Troullier, K. Wu, and Y. Saad, Phys. Rev. B **50**, 11355 (1994).
[23] J. P. Perdew and A. Zunger, Phys. Rev. B **23**, 5048 (1981).
[24] N. Troullier and J. L. Martins, Phys. Rev. B **43**, 1993 (1991).
[25] L. Kleinman and D. M. Bylander, Phys. Rev. Lett. **48**, 1425 (1982).
[26] H. J. Lüdde and R. M. Dreizler, J. Phys. B **16**, 3973 (1983).
[27] Q. Chen, X. H. Ren, S. S. Pu, and F. Wang, J. Phys. B **38**, 4291 (2005).
[28] L. I. Pivovar, M. T. Novikov, and V. M. Tubayev, Zh. Eksp. Teor. Fiz. **42**, 1490 (1962).
[29] M. B. Shah and H. B. Giboby, J. Phys. B **7**, 256 (1974).
[30] J. E. Bayfield and G. A. Khayrallah, Phys. Rev. A **11**, 920 (1975).
[31] N. V. de Castro Faria, F. L. Freire, and A. G. de Pinho, Phys. Rev. A **37**, 280 (1988).
[32] V. V. Afrosimov, D. F. Barash, A. A. Basalaev, N. A. Gucshina, K. O. Lojkin, V. K. Nikulin, M. N. Panov, and I. Yu. Stepanov, Zh. Eksp. Teor. Fiz. **104**, 3297 (1993).
[33] R. A. Baragiola and I. B. Nemirivsky, Nucl. Instrum. Methods **110**, 511 (1973).
[34] V. S. Nikolaev, L. N. Fateyeva, I. S. Dmitriev, and Ya. A. Teplova, Zh. Eksp. Teor. Fiz. **41**, 89 (1961).
[35] R. D. Dubois, Phys. Rev. **33**, 1595 (1986).
[36] T. Kirchner, M. Horbatsch, H. J. Lüdde, and R. M. Dreizler, Phys. Rev. A **62**, 042704 (2000).
[37] L. H. Andersen, P. Hvelplund, H. Knudsen, S. P. Moller, A. H. Sorensen, K. Elsener, K. G. Rensfelt, and E. Uggerhoj, Phys. Rev. A **36**, 3612 (1987).